Revue des Composites et des Matériaux Avancés-Journal of Composite and Advanced Materials
Vol. 35, No. 6, December, 2025, pp. 1189-1197
Journal homepage: http://iieta.org/journals/rcma

Effects of Sustainable Iraqi Porcelanite Waste Powder on the Properties of Commercial Porcelain Tiles

Ishraq Abdalkareem Kalaf Alogaidi[1,2], Ahmed Hafedh Mohammed Mohammed[3], Khairul Anuar Shariff[1*], Hasmaliza Mohamad[1], Muhamed Abdul Fatah Muhamed Mukhtar[1]

[1] School of Materials and Mineral Resources Engineering, Engineering Campus, Universiti Sains Malaysia, Penang 14300, Malaysia
[2] Baghdad Central Laboratory, National Center for Construction Laboratories, Ministry of Construction, Housing and Public Municipalities, Baghdad 10045, Iraq
[3] Department of Materials Engineering, College of Engineering, Mustansiriyah University, Baghdad 10045, Iraq

[*]Corresponding Author Email: biokhairul@usm.my

https://doi.org/10.18280/rcma.350618

Received: 22 October 2025
Revised: 28 November 2025
Accepted: 19 December 2025
Available online: 31 December 2025

Keywords:
Iraqi porcelanite, porosity, mullite, construction materials, MOR

ABSTRACT

Iraqi porcelanite is abundant and exhibits favourable properties, making it a promising sustainable waste resource for engineering applications. This work investigates the influence of waste Iraqi porcelanite on the composition, thermal behaviour and mechanical performance of porcelain tiles. A commercial porcelain formulation was modified by incorporating different porcelanite waste contents. The mixtures were milled at 60 rpm for 24 hours, uniaxially pressed at 35 MPa with a 5-minute dwell time, and sintered at 1200°C for 6 hours at 5°C/min. Chemical and phase compositions of the sintered tiles were characterised by X-ray fluorescence (XRF) and X-ray diffraction (XRD). Thermal conductivity was measured using a Hot Disk Thermal Constants Analyzer, while flexural strength was obtained from three-point bending tests. Adding 1 wt.% porcelanite waste to the commercial formulation reduced thermal conductivity and enhanced fired shrinkage, bulk density and modulus of rupture (MOR) compared with the reference tile. Increasing the porcelanite content to 10 wt.% lowered MOR to 57.99 MPa. Overall, porcelanite-containing tiles remained within typical ranges for commercial porcelain standards, demonstrating an effective route to valorise Iraqi porcelanite waste into high-quality, sustainable construction products. The findings highlight both environmental benefits and technical feasibility for large-scale industrial implementation in Iraq.

1. INTRODUCTION

Porcelanite is a distinct mineral with widespread distribution, particularly in Iraq, where it has attracted considerable interest [1]. This sedimentary mineral phase is composed mostly of Opal CT, an interstratified phase of cristobalite-tridymite, which was derived from biogenic opal, largely associated with diatoms. This sediment is a main component of the Maastrichtian phosphorite series in the Digma Formation, as well as the Akaashat Formation, in the Western Desert [2]. Formed under pressure and temperature [3], porcelanite is converted from rock to clay, contributing to Iraq's diverse geological rock formations. The abundance of porcelain waste in Iraq presents valuable opportunities for various industries, including construction, ceramics, and refractory materials. Its inherent durability, heat resistance, and resistance to chemical corrosion make Iraqi porcelanite highly suitable for various engineering applications [4]. Studies have demonstrated the practical use of porcelanite. For instance, Abrahiam and Abbas [5] found that concrete mix designs with Portland-porcelanite cement, as a supplement to ordinary Portland cement, produced a remarkable increase in their compressive strengths: up to 15% at 28 days and 16.3% at 90 days, compared with controls, for a supplement level of 10%, and by 4% at 28 days with a further increase of 6% at 90 days for a supplement level of 20%. However, Al-Mamoori et al. [6] designed lightweight structural concrete with the addition of porcelanite powder, with concrete densities of less than 2000 kg/m³, self-weight reduced by 25% to as much as 27.4% compared with natural aggregate concrete, with cylindrical compressive strengths of 25.3–36.1 MPa at 28 days. Furthermore, Zinad et al. [7] evaluated varying weight ratios of porcelanite and lithium metasilicate and identified that a 50:50 by weight mix significantly improved the properties of the mixture, such as cold crushing strength and microhardness, indicating its potential for veneer applications. Considering the excellent properties of Iraqi porcelanite, this study investigates the influence of Iraqi porcelanite waste powder utilisation as a sustainable waste-derived raw material in porcelain tile production. Therefore, the main objective of

this study is to systematically evaluate the influence of Iraqi porcelanite waste powder, used as a partial replacement in a commercial porcelain tile formulation, on the compositional, thermal, and mechanical properties of porcelain tiles. It was anticipated that the incorporation of Iraqi porcelanite as an alternative waste material into the ceramic formulation would yield new porcelain tiles with enhanced mechanical properties, particularly higher MOR values and reduced thermal conductivity, due to the Newly developed phases within the sintered tiles. This study demonstrates that Iraqi porcelanite waste can be successfully integrated into commercial porcelain tile production while introducing multiple original findings. The research conducts a complete evaluation of how waste porcelanite affects porcelain tile chemistry through XRF, XRD, Scanning Electron Microscopy (SEM) and porosity measurements which lead to mechanical property improvements and thermal conductivity reductions. The research investigates porcelain tile production with porcelanite waste addition to find the 1 wt.% range which produces maximum densification and bending strength while maintaining thermal conductivity within industrial standards. The research demonstrates a practical method to convert Iraqi waste porcelanite into high-performance porcelain tiles with low thermal conductivity through industrial-scale tile production.

2. MATERIALS AND METHODS

2.1 Fabrication of porcelain ceramic tiles containing Iraqi porcelanite waste powder

The new ceramic tiles were prepared using various raw materials, including Ball clay, China clay (Timex Kaolin Corporation Sdn. Bhd.), Feldspar (Sibelco Malaysia Sdn. Bhd.), Bentonite, and Silica. These components were sourced from the workshop of the School of Materials and Mineral Resources Engineering (SMMRE), Universiti Sains Malaysia (USM), Malaysia. The Iraqi porcelanite waste powder was obtained from the Ministry of Industry and Minerals, General Company for Geological Survey and Mining in Baghdad, Iraq, and incorporated into the ceramic formulation. In total, six different compositions were fabricated, labelled as A, B, C, D, E, and F, with porcelanite waste powder amounts of 0, 1, 3, 5, 7, and 10 wt.%, respectively. Porcelanite waste powder was used as a partial substitute for the ball clay in the porcelain tile formulation because both substances are fine-grained, highly plastic sedimentary clays that typically display a light or near-white colour after firing [6]. Table 1 summarises the specific ceramic tile formulations incorporating Iraqi porcelanite. The raw constituents were uniformly mixed and milled to produce a fine powder using a milling machine at 60 rpm for 24 hours. After milling, 35 g of the powder was uniformly distributed onto a mould surface and sprayed three times with distilled water. The powder was then pressed into a rectangular shape (100 mm × 40 mm × 5 mm) using an Enerpac XLP756XA12GU Workshop Hydraulic Pressing machine with pressure of 75 tonnes. Subsequently, the pressed tiles were sintered at 5°C/min to 1200°C, then soaked for 6 hours in a Carbolite RHF 1600 furnace. After sintering, the specimens were allowed to cool inside the furnace to room temperature (25°C). The sintered tiles were then characterised using various techniques including physical observation, XRF, XRD, SEM, fired shrinkage, bulk density, water absorption, apparent porosity, thermal conductivity and MOR test [8]. The performance and properties of the fabricated porcelain tiles were compared to those of commercial porcelain tiles.

Table 1. The different formulations of the green bodies containing varying amounts of porcelanite waste powder

Raw Material	Weight Percentage (wt.%)						
	Control	A	B	C	D	E	F
China clay	*Commercialised porcelain tile formulation	32	32	32	32	32	32
Ball clay		22	21	19	17	15	12
Feldspar		34	34	34	34	34	34
Bentonite		6	6	6	6	6	6
Silica		6	6	6	6	6	6
Iraqi porcelanite		0	1	3	5	7	10

*This commercialised tile formulation was provided by an industrial collaborator who has opted not to be listed among the authors and affiliations.

2.2 Physical observation

Physical observation test was performed by observing the noticeable colour changes and physical bend, curvature or warping that has occurred to the porcelain tiles after firing. The test is done to determine any major physical changes that may be depicted through the different compositions. The test is done by observing the fired tiles closely using the naked eyes and by comparing them to a standard properly fired tile using the control composition.

2.3 Elemental analysis using XRF

XRF analysis was conducted using a Rigaku ZSX Primus II XRF machine (Tokyo, Japan) to determine the elemental presence of each sample. Prior to undergoing XRF analysis, post-firing tiles were crushed by using a cone crusher (Marcy Gy-Roll Crusher, U.S.A.) and followed by milling for 3 minutes in a ring mill machine to get a uniform and fine powder then sieved through a 75 μm sieve.

2.4 Compositional analysis using XRD

The presence of a compositional phase in the fired specimens was detected using an XRD (Model: Bruker AXS D8 Advance). Post-firing tiles were crushed into powder form and analysed at 40 kV and 40 mA, with the diffraction angle (2θ) set within the range of 10–90°. These phases were identified using comparison with standard reference diffraction patterns provided by the International Centre for Diffraction Data (ICDD) as their reference, with the diffraction spectra analyzed with the use of the X'Pert HighScore Plus computer program. In addition, the software INEL-EQUNIX 3000, French, was applied to determine phase composition [9].

2.5 Cross-section morphological analysis

The fired specimens with varying compositions of Iraqi porcelanite were cut with a dimension (10 × 10) mm by using variable speed diamond cutter (Model: VSD-3000), and then attached to a piece of carbon tape before being coated with a layer of gold-palladium for a 5-minute under vacuum conditions using SEM coating system (Model: E5550 BIO-RAD Polaron Division, Stafford, United States). Then, the cross-section morphology of the specimens was observed using a TM-3000 SEM (Hitachi High Technologies Co., Tokyo, Japan) at 500X, 1000X, and 2000X magnification [10].

2.6 Fired shrinkage analysis

Fired shrinkage is a key parameter for controlling the final product size. International Organization for Standardization ISO 13006 outlines the quality standards for ceramic tiles, including requirement for dimensional variation during production. Prior to the firing shrinkage analysis, three rectangular test samples (100 mm × 40 mm × 5 mm) were prepared using 35 g of mixture from each composition listed in Table 1. The samples were compacted at 35 MPa, sintered at 5°C/min to 1200°C, soaked for 6 hours, and cooled to room temperature (25°C) inside a furnace. Subsequently, the firing shrinkage of the ceramic tiles was determined based on the volume change according to ISO 10545-2, as shown in Eq. (1):

$$\text{Fired shrinkage (\%)} = [(V_1-V_2)/V_1] \times 100\% \quad (1)$$

where, V_1 and V_2 denote the dry and fired volumes of the ceramic tiles (cm^3), respectively.

2.7 Bulk density

Bulk density is the ratio of a material's mass to its total volume, including particles, voids, and internal pores. Since the bulk density of a material varies based on its components, composition, and the void spaces present, it is not considered an intrinsic property. In view of this, these requirements determine the dry mass and structural dimensions of each sample [11]. In this study, the weight of three samples was determined for each mixture with the use of an analytical balance, and the bulk density of the mixtures was determined as the mean of the three. Bulk density was determined through the use of ISO 10545-3, using Eq. (2) as follows:

$$\text{Bulk density} = M_1/V \quad (2)$$

where, M_1 and V denote the dry mass (g) and volume of the fired ceramic tile (cm^3), respectively.

2.8 Water absorption

The water absorption capacity (wt.%) of the fired ceramic tiles was determined through the immersion method, as defined in ISO 10545-3. Before being immersed in water, the test pieces were dried initially until their masses were constant. After that, immersion was carried out for a further 24 hours, giving the water absorption value. The water absorption percentage was then determined using Eq. (3) as follows:

$$\text{Water absorption (\%)} = [(M_2–M_1)/M_1] \times 100\% \quad (3)$$

where, M_1 and M_2 refer to the dry and soaked masses of fired ceramic tile (g), respectively.

2.9 Apparent porosity

The apparent porosity of the fired tiles was determined in accordance with ISO 10545-3. This calculation value represents the percentage of open porosity in the fired tiles relative to their external volume. Data for this assessment was recorded during the water absorption test. Eq. (4) was used to estimate the apparent porosity:

$$\text{Apparent porosity (\%)} = [(M_2– M_1)/V] \times 100\% \quad (4)$$

where, M_1 and M_2 denote the dry and soaked masses of the fired ceramic tile (g), respectively, and V refers to the fired ceramic tile volume (cm^3).

2.10 Fired MOR

The Fired MOR measurements were employed to evaluate the fabricated fired ceramic according to ISO 10545-4. A Macklow-Smith MST433 testing machine (Macklow-Smith Engineering Ltd., Surrey, United Kingdom) was employed for finding the MOR of the samples through three-point bending with a crosshead speed of 5 mm/min, as well as the load cell capacity of 5 kN. Before the test was carried out, the dimensions of the length, width, and thickness of the fired porcelain tiles were determined in order for them to meet the desired geometric requirements. Once the sample is placed in the centre of the MOR machine, a load is applied at 90° to the sample surface, specifically at the midpoint between the supporting pins [12]. Eq. (5) was applied to quantify the MOR of the fired tiles:

$$\text{MOR} = 3FL/2bd^2 \quad (5)$$

where, F is the force at fracture (N), L is the distance between the support rollers (mm), b is the width of the tile (mm), and d is the tile thickness (mm).

2.11 Thermal conductivity

Thermal conductivity is a property of materials that defines the rate at which heat energy is transferred through them. It is measured in watts per meter-kelvin W/(m·K). A Hot Disk Thermal Constants Analyzer (TPS 2500, Hot Disk AB, Sweden) was used to measure the thermal conductivity of the fired ceramic tiles. Before testing, the sample must be at least 2 cm in length and width and have a sufficiently smooth surface to ensure proper contact with the sensor during the thermal conductivity measurement. The ceramic tile was broken into two pieces, and a flat Hot Disk sensor was placed between them, with the front surfaces of the tiles facing the sensor. Thermal conductivity testing was conducted at a temperature of 25°C using a power input of 0.5 watts for a duration of 5 seconds, by recording the temperature as a function of time response in the sensor.

2.12 Statistical analysis

Quantitative data are presented as mean values together with their standard deviations. Comparisons between the different porcelain tile compositions were performed using

one-way ANOVA. Statistical significance was interpreted using the following thresholds: *** $p < 0.01$, ** $p < 0.05$, * $p < 0.1$ and n.s. = nonsignificant.

3. RESULTS AND DISCUSSION

3.1 Physical appearance

Figure 1 depicts the physical appearance of the fired porcelain tiles. Visual observation revealed that the colour of all fired tiles was nearly identical. The compositions of the colouring agents (Fe_2O_3 and TiO_2), as determined by XRF analysis, were 6.47 wt.% and 1.21 wt.% (sample A), 5.54 wt.% and 1.15 wt.% (sample B), 4.80 wt.% and 1.02 wt.% (sample C), 3.86 wt.% and 0.94 wt.% (sample D), 4.47 wt.% and 1.05 wt.% (sample E), and 4.29 wt.% and 1.04 wt.% (sample F), respectively. In particular, Fe_2O_3, a key colouring agent, can alter the colour of the porcelain by reacting with SiO_2 and Al_2O_3 to form red-coloured hematite [13]. The image also indicates increasing warpage of the porcelain tiles from samples A to F. Warpage that occurs as a result of firing is mostly related to the formation of a liquid phase as the percentage of flux oxides (for example, K_2O, MgO, CaO) rises. With the rising percentage of this liquid phase, warpage becomes more noticeable as the percentage of flux rises [14].

3.2 Elemental XRF analysis

Table 2 summarises the elemental compositions of samples A–F after the firing process. After firing, sample A (0 wt.%) recorded the lowest SiO_2 level at 55.1 wt.% and the highest amount of Al_2O_3 at 25.9 wt.%. The SiO_2 and Al_2O_3 compositions served as an Al-Si precursor to form the mullite phase during firing above 1200°C through the reaction between silica and alumina. The ideal Al_2O_3/SiO_2 molar ratio for the mullite phase formation is 3:2 [15]. For instance, sample A recorded an Al_2O_3/SiO_2 ratio of 0.47, indicating an excess amount of silica. The role of SiO_2 is crucial in ceramics, as it contributes to the formation of an amorphous quartz phase that facilitates pore size reduction in sintered tiles.

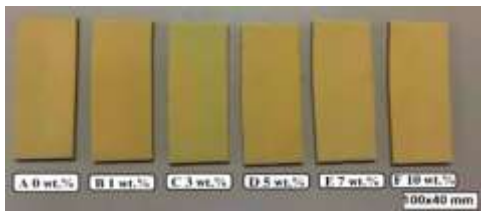

Figure 1. Physical appearance of fired porcelain tiles containing different porcelanite waste contents (A: 0 wt.%, B: 1 wt.%, C: 3 wt.%, D: 5 wt.%, E: 7 wt.%, F: 10 wt.%) after firing at 1200°C

Table 2. XRF-determined chemical oxide composition (wt.%) of all samples after firing

Element	After Firing					
	A (0 wt.%)	B (1 wt.%)	C (3 wt.%)	D (5 wt.%)	E (7 wt.%)	F (10 wt.%)
SiO_2	55.1	55.5	58.5	59.0	61.0	61.3
Al_2O_3	25.9	23.9	23.4	22.4	21.9	21.5
Fe_2O_3	6.47	5.54	4.80	3.86	4.47	4.29
TiO_2	1.21	1.15	1.02	0.94	1.05	1.04
K_2O	10.8	10.2	9.76	9.20	9.30	9.10
CaO	1.02	1.04	1.06	1.10	1.30	1.46
MgO	1.00	2.00	3.00	3.60	3.60	4.00
P_2O_2	0.40	0.50	0.90	0.60	0.70	0.40
Al_2O_3/ SiO_2 ratio	0.47	0.43	0.40	0.38	0.36	0.35
Total alkaline content	12.8	13.0	13.8	13.9	14.2	14.6

In addition, sample A contains a significant amount of fluxing element (K_2O), approximately 10.8 wt.% higher compared to other samples. These fluxing oxides promote a highly fluid glassy phase during firing, which in turn enables the ceramic body to be sintered at lower temperatures [16]. Furthermore, sample A exhibits the highest content of colouring oxides, with 6.47 wt.% Fe_2O_3 and 1.21 wt.% TiO_2, affecting the final tile colour. A high amount of Fe_2O_3, for example, reacts with SiO_2 and Al_2O_3 to form a hematite phase, yielding a red hue [17].

Samples B through F show increasing amounts of SiO_2, which were determined from the XRF results presented in Table 2, with compositions of 55.5 wt.%, 58.5 wt.%, 59.0 wt.%, 61.0 wt.%, and 61.3 wt.%, respectively. The increasing trend is due to the elevated addition of Iraqi porcelanite waste powder in the tile formulation. The XRF analysis showed that the raw material contains 78.4 wt.% SiO_2. In contrast, samples B, C, D, E, and F recorded reduced Al_2O_3 concentrations of 23.9 wt.%, 23.4 wt.%, 22.4 wt.%, 21.9 wt.%, and 21.5 wt.%, respectively. The findings indicate a decline in the Al_2O_3/SiO_2 ratio in each sample at 0.43, 0.40, 0.38, 0.36, and 0.35, respectively, compared to sample A, which affected the mullite phase formation [18]. As the amount of Iraqi porcelanite increased, the new body compositions of samples B, C, D, E, and F exhibited relatively lower K_2O concentrations and higher CaO and MgO levels compared to sample A. Notably, K_2O content showed a decreasing trend, while CaO and MgO content increased across the samples. Hence, these variations influence phase formation and liquid-phase viscosity during the firing process [19].

3.3 Compositional analysis

Figure 2, as well as Table 3, illustrate the XRD patterns and the associated phase composition derived from the Rietveld refinement of all compositions containing different amounts of Iraqi porcelanite waste powder. Quartz and mullite are the dominant crystalline phases in all samples. With increasing porcelanite content, the relative intensity of mullite increases while quartz decreases, indicating enhanced mullitization after firing.

In all compositions, Quartz (SiO_2) and Mullite ($3Al_2O_3 \cdot 2SiO_2$) were found, which agreed well with Amigó et al. [20], thus proving their existence within the compositions

presented. In addition, a high fraction of amorphous glassy phase, around 61.26%, was quantified in sample F.

The mullite phase formation is significantly affected by the Al_2O_3/SiO_2 ratio in the raw materials. Hence, maintaining an Al_2O_3/SiO_2 ratio of close to 3:2 is recommended to achieve optimal mullite phase formation that matches the stoichiometry of $3Al_2O_3 \cdot 2SiO_2$ [16]. A higher Al_2O_3/SiO_2 ratio promotes greater mullite phase formation due to the increased availability of Al_2O_3 for dissolution during firing, thus enhancing the nucleation of mullite crystals [21].

However, the samples in this study exhibited a decreasing Al_2O_3/SiO_2 ratio, as indicated in Table 2. Furthermore, Table 3 shows that a slight increase in the mullite phase formation from samples A to C can be attributed to the elevated presence of alkaline earth oxides (K_2O, MgO, and CaO). These oxides served as fluxing agents, lowering melting points and facilitating more liquid phase formation. Consequently, the increased amounts of dissolved silica interacting with the Al-Si spinel in the phase resulted in a relatively higher generation of mullite phase. Likewise, the excessive addition of fluxing agents may impede the formation of the mullite phase because the excess flux disrupts Al_2O_3-SiO_2 balance, increases glass phase, hinders mullite crystallization, and weakens mechanical properties [22]. In comparison, the slight reduction in the mullite phase in sample D (15.35 wt.%) than in sample C (16.57 wt.%) was attributed to the presence of metal oxides, such as MgO, that hindered the formation of new mullite phase [23]. The higher amount of MgO can also gradually convert the mullite phase into spinel ($MgAl_2O_4$). This spinel phase dissolves into the glass phase when exposed to a firing temperature of 1200°C and a prolonged soaking duration of 6 hours. Furthermore, a decrease in the presence of the quartz phase corresponding to an increase in the amorphous glass phase from samples A to F. The shift from the quartz phase, which is a result of unreacted silica in the tiles [24], toward the amorphous glass phase is due to the quartz dissolution into the amorphous glass during the firing process [25]. The amorphous glass phase formation also relies on the amount of fluxing agent in the composition. Notably, an increase in alkaline oxide contents (K_2O, MgO, and CaO) was recorded at 12.8 wt.%, 13 wt.%, 13.8 wt.%, 13.9 wt.%, 14.2 wt.%, and 14.6 wt.% from samples A to F, respectively. This increased addition of fluxing agents led to excess dissolution of SiO_2 into the glass due to its lower melting point. Consequently, some SiO_2 particles remained in their quartz state, leading to a higher proportion of the amorphous glass phase in the samples as the quartz phase diminished.

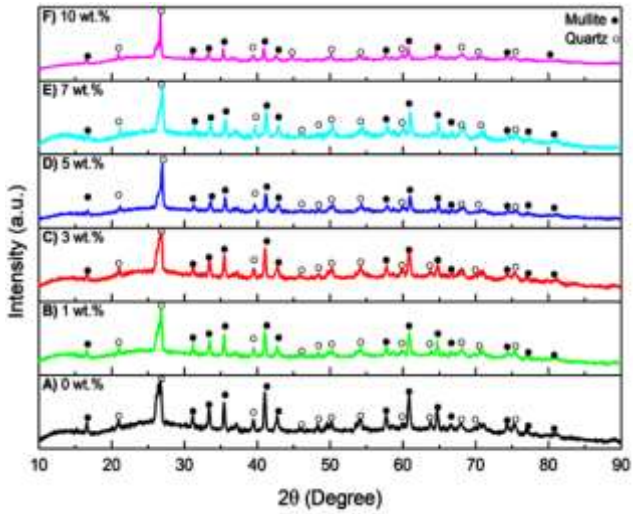

Figure 2. The XRD patterns of samples A, B, C, D, E, and F after firing at 1200°C

Table 3. Phase composition (%) of the fired samples based on the Rietveld refinement method

Sample (wt.%)	Chapter 1 Quartz	Chapter 2 Mullite	Chapter 3 Amorphous Glass Phase
A (0)	Chapter 4 29.20	Chapter 5 14.66	Chapter 6 56.14
B (1)	Chapter 7 27.50	Chapter 8 15.67	Chapter 9 56.83
C (3)	Chapter 10 26.71	Chapter 11 16.57	Chapter 12 56.72
D (5)	Chapter 13 25.39	Chapter 14 15.35	Chapter 15 59.25
E (7)	Chapter 16 25.11	Chapter 17 14.69	Chapter 18 60.20
F (10)	Chapter 19 24.64	Chapter 20 14.10	Chapter 21 61.26

3.4 Morphological analysis

Figure 3 displays the cross-sectional morphology of all samples after firing at 1200°C. Although all samples exhibited pores (black holes), as highlighted with red circles in the captured images, their numbers vary among the samples. For example, sample C (3 wt.% Iraqi porcelanite) recorded the lowest porosity, suggesting effective pore closure and densification during firing. The reduced porosity in samples A to C is linked to the formation of the liquid phase during firing, facilitated by fluxing agents (K_2O, MgO, and CaO). This liquid phase fills the pores via capillary action, facilitating particle rearrangement and densification. Besides, the increase in alkaline oxides across the samples correlates with the higher content of Iraqi porcelanite waste powder, which is rich in CaO and MgO (4.61 wt.% and 8.70 wt.%). Conversely, samples D, E, and F achieved greater porosity compared to sample C, implying potential issues related to excessive liquid phase formation.

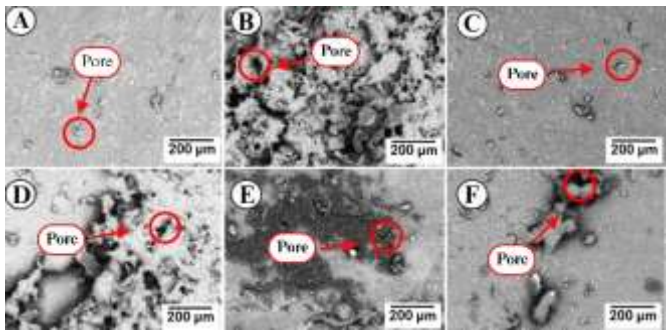

Figure 3. Cross-section SEM images of the tile samples containing varying proportions of Iraqi porcelanite waste powder in ceramic tile formulation: (A) 0 wt.%, (B) 1 wt.%, (C) 3 wt.%, (D) 5 wt.%, (E) 7 wt.%, and (F) 10 wt.%
Note: Cross-sectional images under 500X magnification

During firing at 1200°C, the ceramic tiles exhibited extensive atomic diffusion and liquid-phase formation,

promoted by fluxing oxides such as K_2O, CaO, and MgO. The transient liquid phase infiltrated the pores by capillary forces, enabling particle rearrangement, neck formation, and grain growth. These mechanisms collectively facilitated densification and pore closure, transforming the microstructure into a denser glassy–ceramic matrix with reduced porosity and improved mechanical strength [26].

3.5 Fired shrinkage and bulk density

Figure 4 presents the firing shrinkage and bulk density values for all tile specimens after firing. In general, samples A to C show an increasing trend in both shrinkage and bulk density, while samples C to F exhibit a decreasing trend. Phase formation can influence these properties after firing. In terms of liquid phase formation, increased mullite phase content leads to greater shrinkage. According to Table 3, the mullite phase content gradually increases from samples A to C, peaking at 16.57% for the latter. The reaction between the Al-Si spinel phase and amorphous silica forms the mullite phase, which expanded the volume by 10% during cooling, eliminating any voids or cracks caused by shrinkage and expansion [27].

Consequently, the increase in mullite phase content in samples A to C correlates with the increased shrinkage and bulk density.

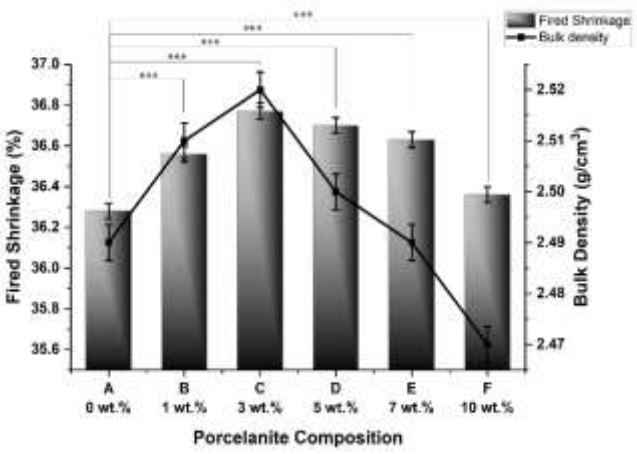

Figure 4. Fired shrinkage and bulk density of tiles containing different proportions of porcelanite waste powder after sintering at 1200℃ (*** $p < 0.01$)

Also, from Figure 3 (samples A–C) the reduced porosity is also attributed to the liquid phase formation during firing. Conversely, the slight decline in mullite phase content in sample C (16.57%) to sample F (14.10%) resulted in densification and reduced shrinkage [28]. Therefore, to elucidate the effect of porosity on the bulk density and fired shrinkage of the specimens, water absorption and apparent porosity are discussed in the following section.

3.6 Water absorption and apparent porosity

The water absorption and apparent porosity of the fired ceramic tiles are depicted in Figure 5. Accordingly, both properties exhibit a similar progressive decrease from samples A to C and a slight increase from samples C to F. Sample F exhibited the highest water absorption and apparent porosity of 1.17% and 2.99%, respectively, while sample C recorded the lowest water absorption and apparent porosity of 0.76% and 1.90%, respectively. Water absorption of samples D, E, and F increased with a more significant number of open pores, which aligns with the SEM results in Figure 3. Since water absorption is quantified based on sample weight; therefore, a sample with a low density due to high porosity is expected to possess a high-water adsorption [29]. While decreasing porosity results in diminished water absorption, as observed in samples A to C, increasing porosity leads to slightly higher water absorption in samples C to F. The SEM results in Figure 3 supported this finding, which shows a reduction in pore numbers from samples A to C. From the calculated values, there is a remarkable reduction in the value of apparent porosity from samples A through B, down to sample C, as shown in Figure 5. On the other hand, the water absorption as well as apparent porosity increase once again in samples D, E, and F compared to that of sample C due to a higher degree of pore development.

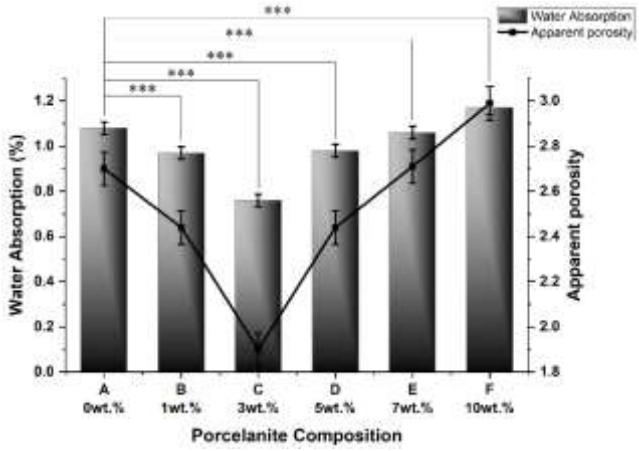

Figure 5. Water absorption and apparent porosity of tiles containing different porcelanite waste contents after firing at 1200℃ (*** $p < 0.01$)

Based on Figure 5, water absorption decreases from samples A to C due to the reduction in pore numbers. This is further proven by the fired shrinkage results in Figure 4, which highlight a lower number of pores in these samples. The result is also consistent with the calculated apparent porosity values, which decrease from samples A to C (Figure 5). Conversely, water absorption and apparent porosity for samples D, E, and F improved compared to sample C due to the higher pore formation, in line with the fired shrinkage results in Figure 4. Since all samples exhibit water absorption below 1%, they can be considered porcelain tiles based on industry standards [30, 31].

3.7 Modulus of rupture of specimens

As shown in Figure 6, the MOR value of the fired ceramic tiles rises initially from Sample A (59.99 MPa) to Sample C (61.91 MPa) and then falls from Sample C (61.91 MPa) through Sample D (61.58 MPa), Sample E (58.69 MPa), and Sample F (57.99 MPa).

The higher mullite phase content correlates with the increased bending strength in ceramic tiles. The bending strength of fired ceramic tiles is affected by two key factors: porosity and phase composition. During firing, the pores formed within the tile bodies act as local stress concentrators. These regions of concentrated stress facilitate crack initiation and propagation, thereby reducing the overall mechanical

strength of the fired ceramics. Therefore, the MOR values of samples A to C increase due to the decreased porosity, as shown in the SEM (Figure 3) and apparent porosity (Figure 5). In contrast, the MOR value of samples D, E, and F decreases compared to sample C as the porosity increases slightly, as shown in the SEM (Figure 3) and apparent porosity (Figure 5). The phase composition of the fired ceramics also has a strong influence on their final bending strength. In particular, the mullite phase plays a critical role in improving the MOR. As a crystalline phase, mullite exhibits desirable properties such as low thermal expansion, relatively low thermal conductivity, and high fracture strength and toughness, which make it especially beneficial for ceramic tile applications [32].

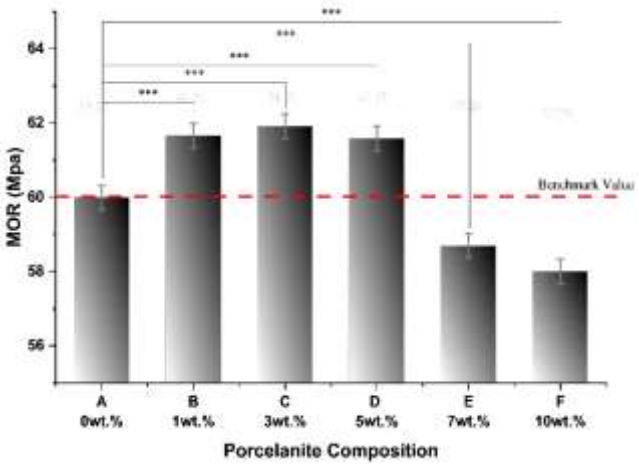

Figure 6. Comparison of MOR values for fired porcelain tiles incorporated with varying compositions of Iraqi porcelanite after firing at 1200°C (*** $p < 0.01$)

Notably, the overall MOR values of all ceramic tiles in this study are relatively high compared to commercial ceramic tiles, which typically exhibit MOR values above 27 MPa [21]. The homogeneity of the ceramic tiles, which refers to the consistency of the tile's composition and structure, also influences their MOR values. Greater homogeneity generally results in higher MOR values, as it minimizes variability in the material's properties as shown in scanning electron microscope SEM (Figure 3C) with 3 wt.% porcelanite waste powder, homogeneity occurred because a liquid phase enhanced the diffusion of particles and helped eliminate pores, reduce gradients in composition, and smooth out irregularities in the microstructure, resulting in a more uniform appearance. On the contrary, agglomeration can adversely impact MOR through the emergence of weak points in the tile, reducing its strength and hardness that can be shown in SEM (Figure 3B, D, E and F). Thus, both homogeneity and agglomeration are essential parameters of the mechanical performance of ceramic tiles. Although samples B, C, and D remain above the Benchmark MOR (sample A) but thermal conductivity needs to be elucidated and discussed in the next section.

3.8 Thermal conductivity

The thermal properties for all fired ceramic tiles are shown in Figure 7. Based on Figure 7, the thermal conductivity values exhibit an upward trend from sample A (1.360 W/(mk)) to sample C (1.389 W/(mk)), followed by a steady reduction from sample C (1.389 W/(mk)) to samples D (1.331 W/(mk)), E (1.140 W/(mk)), and F (1.142 W/(mk)). There are many factors that affect thermal conductivity, such as the presence of pores and their shape, mineralogical composition [33, 34]. In terms of phase presence, XRD results indicated that sample A had the highest amount of quartz (29.20%) and notable amount of mullite (14.66%) as shown in Table 3. These two phases have a high thermal conductivity 4.7 W/(m.k) for mullite and 6.2 W/(m.k) for quartz [35], which may contribute to an increase in the thermal conductivity of the ceramic tiles. Meanwhile, Samples B, D, E and F exhibited relatively lower thermal conductivity compared to sample A, which may be associated with the reduced quartz amounts (27.50%, 25.39%, 25.11% and 24.64%, respectively). While the thermal conductivity of sample C increased, which was attributed to the lower porosity, as evidenced by SEM (Figure 3), apparent porosity (Figure 5) and MOR (Figure 6).

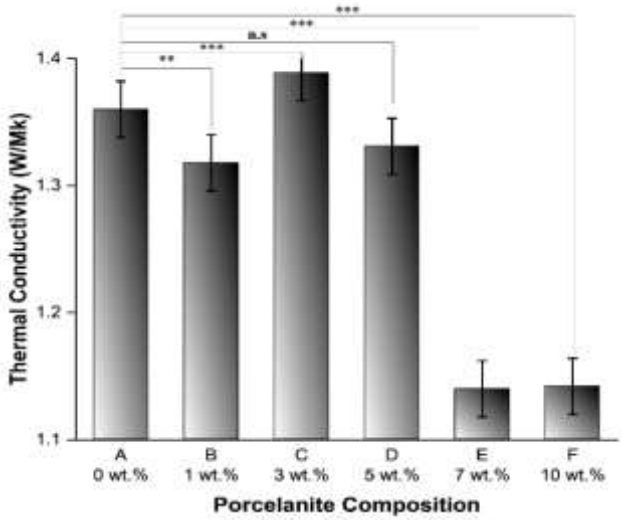

Figure 7. Comparison of thermal conductivity values of ceramic tiles incorporated with varying compositions of Iraqi porcelanite after firing at 1200°C (*** $p < 0.01$, ** $p < 0.05$, and n.s = insignificant)

4. CONCLUSIONS

4.1 Conclusions

The research shows that adding Iraqi porcelanite waste powder to commercial porcelain tile materials produces beneficial changes in phase structure and microstructure which lead to better mechanical and thermal properties. The study finds that adding 1% porcelanite waste to the tile mixture gives the best results because it improves fired shrinkage and bulk density and MOR while decreasing thermal conductivity compared to the reference tile. The addition of more than 7% porcelanite waste results in excessive glass formation and pore development which cause MOR values to decrease; however, the produced tiles meet commercial porcelain body standards. The research demonstrates that Iraqi porcelanite waste serves as an environmentally friendly alternative material for creating porcelain tiles with enhanced characteristics and reduced environmental impact.

4.2 Limitations and future work

The present work is limited to one firing schedule (1200°C, 6 hours) and a relatively narrow porcelanite addition range (0–

10 wt.%). In addition, only room-temperature properties (shrinkage, density, water absorption, MOR and thermal conductivity) were evaluated at the lab scale, without long-term durability, wear, or thermal-shock testing, and without a full techno-economic or life-cycle assessment.

Future work should investigate a wider porcelanite-content range and multiple firing temperatures, assess long-term durability (abrasion, frost, thermal shock), and combine microstructural characterisation with modelling to quantify the roles of mullite, glassy phase, and porosity. This will further support large-scale industrial implementation.

ACKNOWLEDGMENTS

The corresponding author would like to thank National Baghdad Central Laboratory, National Center for Construction Laboratories, Ministry of Construction, Housing and Public Municipalities, Baghdad, Iraq, General Company for Geological Survey and Mining, Ministry of Industry and Minerals, in Baghdad, Iraq, for porcelanite waste powder. Also, to Dr. Ahmed Hafedh Mohammed Mohammed from Department of Materials Engineering, College of Engineering, Mustansiriyah University, Baghdad, Iraq for verifying the importance of utilizing porcelanite waste powder as alternative materials to fabricate sustainable construction materials.

REFERENCES

[1] Abood, M.I., Jassim, T.E. (2018). Removal of methylene blue from aqueous solutions using Iraqi porcellanite rocks. World Journal of Pharmaceutical Research, 7(19): 230-243. https://wjpr.s3.ap-south-1.amazonaws.com/article_issue/1543580570.pdf?utm_source=chatgpt.com

[2] Waheed, G.A. (2022). Assessment of the use of various sources of silica on the properties of porcelain. Doctoral dissertation, Babylon University.

[3] Labus, M., Labus, K. (2018). Thermal conductivity and diffusivity of fine-grained sedimentary rocks. Journal of Thermal Analysis and Calorimetry, 132(3): 1669-1676. https://doi.org/10.1007/s10973-018-7090-5

[4] Ahmed, S., Al-Adili, A., Hameed, A. (2022). A short review on preparation and characterization of iraqi porcelanite aggregate concrete. Journal of Applied Sciences and Nanotechnology, 2(1): 49-58. https://doi.org/10.53293/jasn.2021.3565.1028

[5] Abrahiam, A.A., Abbas, Z.K. (2020). Resistance of manufactured blended portland-porcelanite cement to internal sulfate attack. Journal of Engineering Science and Technology, 5: 3344-3354.

[6] Al-Mamoori, F.H., Al-Mamoori, M.H., Najim, W.N. (2018). Production of structural light-weight aggregate concrete using different types of Iraqi local crushed materials as coarse aggregate. Journal of University of Babylon for Engineering Sciences, 26(1): 362-375.

[7] Zinad, R.S., Merzah, A.S., Mohammed, S.K. (2019). Studying the physical and mechanical properties of porcelanite: Lithium metasilicate composite as a dental veneer material. IOP Conference Series: Materials Science and Engineering, 518(3): 032010. https://doi.org/10.1088/1757-899x/518/3/032010

[8] Contartesi, F., Melchiades, F.G., Boschi, A.O. (2019). Anticipated overfiring in porcelain tiles: Effects of the firing cycle and green bulk density. Boletín de la Sociedad Española de Cerámica y Vidrio, 58(2): 69-76. https://doi.org/10.1016/j.bsecv.2018.07.001

[9] Ibrahim, F.A., Kadhim, Z.D., Abdulrazzaq, M.A., Aydi, A. (2025). Effect of Al_2O_3 particle size on mechanical properties of Al-12%Si alloy via taguchi method. Revue des Composites et des Matériaux Avancés-Journal of Composite and Advanced Materials, 35(4): 601-608. https://doi.org/10.18280/rcma.350401

[10] Hussein, I.S., Hassan, N.A., Jassam, M.G. (2025). Effect of initial saturation level on leaching and permeability of treated gyoseous soil. Revue des Composites et des Matériaux Avancés-Journal of Composite and Advanced Materials, 35(4): 619-628. https://doi.org/10.18280/rcma.350403

[11] Liuzzi, S., Rubino, C., Martellotta, F., Stefanizzi, P. (2023). Sustainable materials from waste paper: Thermal and acoustical characterization. Applied Sciences, 13(8): 4710. https://doi.org/10.3390/app13084710

[12] Maid, A.A., Mashrei, M.A. (2025). Investigation the behavior fibrous-RC beams strengthening by CFRP on grooves with different compressive strengths of concrete. Revue des Composites et des Matériaux Avancés-Journal of Composite and Advanced Materials, 35(4): 697-707. https://doi.org/10.18280/rcma.350412

[13] Kostomitsopoulou Marketou, A., Kouzeli, K., Facorellis, Y. (2019). Colourful earth: Iron-containing pigments from the Hellenistic pigment production site of the ancient agora of Kos (Greece). Journal of Archaeological Science: Reports, 26: 101843. https://doi.org/10.1016/j.jasrep.2019.05.008

[14] Dong, W., Bao, Q., Zhou, J., Zhao, T., Liu, K., Hu, Z. (2017). Preparation of porcelain building tiles using "K_2O-Na_2O" feldspar flux as a modifier agent of low-temperature firing. Journal of the Ceramic Society of Japan, 125(9): 690-694. https://doi.org/10.2109/jcersj2.16327

[15] Sánchez-Soto, P.J., Eliche-Quesada, D., Martínez-Martínez, S., Pérez-Villarejo, L., Garzón, E. (2022). Study of a waste kaolin as raw material for mullite ceramics and mullite refractories by reaction sintering. Materials, 15(2): 583. https://doi.org/10.3390/ma15020583

[16] Hanapi, M.I., Ahmad, S., Taib, H., Ismail, A.E., Rahman, M.N.A., Salleh, S.M., Sadikin, A., Mahzan, S. (2017). Influence of alkali resistant (Ar) fibreglass in porcelain clay for manufacturing vitrified clay pipes. Journal of Physics: Conference Series, 914: 012020. https://doi.org/10.1088/1742-6596/914/1/012020

[17] Chen, Y.B., Du, Y., Guo, Y.F., Guo, X.M. (2022). Quantitative investigation of MgO, Al_2O_3 and SiO_2 effects on solid-state formation of secondary hematite in sintering process of iron ore fines. Minerals, 12(3): 282. https://doi.org/10.3390/min12030282

[18] Koshy, P., Ho, N., Zhong, V., Schreck, L., Koszo, S.A., Severin, E.J., Sorrell, C.C. (2021). Fly ash utilisation in mullite fabrication: Development of novel percolated mullite. Minerals, 11(1): 84. https://doi.org/10.3390/min11010084

[19] Boulaiche, K., Boudeghdegh, K., Haddad, S., Roula, A., Alioui, H. (2022). Valorisation of industrial soda-lime glass waste and its effect on the rheological behavior, physical-mechanical and structural properties of sanitary

ceramic vitreous bodies. Annales de Chimie - Science des Matériaux, 46(3): 147-154. https://doi.org/10.18280/acsm.460306

[20] Amigó, J.M., Serrano, F.J., Kojdecki, M.A., Bastida, J., Esteve, V., Reventós, M.M., Martí, F. (2005). X-ray diffraction microstructure analysis of mullite, quartz and corundum in porcelain insulators. Journal of the European Ceramic Society, 25(9): 1479-1486. https://doi.org/10.1016/j.jeurceramsoc.2004.05.019

[21] Romero, M., Padilla, I., Contreras, M., López-Delgado, A. (2021). Mullite-based ceramics from mining waste: A review. Minerals, 11(3): 332. https://doi.org/10.3390/min11030332

[22] Li, Q., Meng, X., Zhang, X., Liang, J., Zhang, C., Li, J., Zhou, Y., Sun, X. (2022). Enhanced 3D printed Al_2O_3 core via in-situ mullite. Additive Manufacturing, 55: 102826. https://doi.org/10.1016/j.addma.2022.102826

[23] Pasiut, K., Partyka, J., Bućko, M.M., Grandys, M., Kurpaska, Ł., Piekarczyk, W. (2020). An impact of the molar ratio of $Na2O/K_2O$ on nanomechanical properties of glaze materials containing zirconium oxide. Journal of Alloys and Compounds, 815: 152411. https://doi.org/10.1016/j.jallcom.2019.152411

[24] Medeiros, P.S.S., Lira, H.L., Rodriguez, M.A., Menezes, R.R., Neves, G.A., Santana, L.N.L. (2019). Incorporation of quartzite waste in mixtures used to prepare sanitary ware. Journal of Materials Research and Technology, 8(2): 2148-2156. https://doi.org/10.1016/j.jmrt.2019.02.001

[25] Ozturk, Z.B., Ay, N. (2018). Investigation of porosity of ceramic tiles by means of image analysis method. Journal of Ceramic Processing Research, 15: 393-397. https://doi.org/10.36410/jcpr.2014.15.6.393

[26] Dixit, P., Rawal, B., Panda, H.S., Kumar, B.P. (2022). Investigation of mechanical properties based on the particle size of alumina ceramics prepared by circulatory bead milling. Ceramics International, 48(19): 29274-29283. https://doi.org/10.1016/j.ceramint.2022.05.218

[27] Islam, R.A., Chan, Y.C., Islam, M. (2004). Structure-property relationship in high-tension ceramic insulator fired at high temperature. Materials Science and Engineering: B, 106(2): 132-140. https://doi.org/10.1016/j.mseb.2003.09.005

[28] Alves, H.P.A., Araújo, A.J.M., Andrade, R.M., Junior, R.A., Ferreira, H.S., Acchar, W., Campos, L.F.A., Macedo, D.A. (2022). Processing of mullite-glass ceramics using simplex-centroid design: Densification process dominated by liquid-phase sintering. Boletín de la Sociedad Española de Cerámica y Vidrio, 61(2): 160-168. https://doi.org/10.1016/j.bsecv.2020.09.002

[29] Dong, Y., Guo, W., Jiang, C., Shao, Y., Zhang, L., Wang, D., Lu, X., Huang, S., Cheng, X. (2023). Using CaO as a modifier agent to optimize the pore structure of foamed ceramics from granite scrap. Ceramics International, 49(9): 13443-13451. https://doi.org/10.1016/j.ceramint.2022.12.219

[30] Pinheiro, B.C.A., Holanda, J.N.F. (2013). Reuse of solid petroleum waste in the manufacture of porcelain stoneware tile. Journal of Environmental Management, 118, 205-210. https://doi.org/10.1016/j.jenvman.2012.12.043

[31] Piccolo, P.O., Zaccaron, A., Teixeira, L.B., de Moraes, E.G., Montedo, O.R.K., de Oliveira, A.P.N. (2022). Development of translucent ceramic tiles from modified porcelain stoneware tile paste. Journal of Building Engineering, 45: 103543. https://doi.org/10.1016/j.jobe.2021.103543

[32] Cui, K., Zhang, Y., Fu, T., Wang, J., Zhang, X. (2020). Toughening mechanism of mullite matrix composites: A review. Coatings, 10(7): 672. https://doi.org/10.3390/coatings10070672

[33] Gualtieri, M.L., Gualtieri, A.F., Gagliardi, S., Ruffini, P., Ferrari, R., Hanuskova, M. (2010). Thermal conductivity of fired clays: Effects of mineralogical and physical properties of the raw materials. Applied Clay Science, 49(3): 269-275. https://doi.org/10.1016/j.clay.2010.06.002

[34] Tian, Z. (2018). Homogenization of mechanical and thermal properties of fired clay bricks: Effects of porosity. Doctoral dissertation, INSA de Toulouse.

[35] Allegretta, I., Eramo, G., Pinto, D., Hein, A. (2017). The effect of mineralogy, microstructure and firing temperature on the effective thermal conductivity of traditional hot processing ceramics. Applied Clay Science, 135: 260-270. https://doi.org/10.1016/j.clay.2016.10.001